Available online at www.sciencedirect.com

jmr&t Journal of Materials Research and Technology

journal homepage: www.elsevier.com/locate/jmrt

Original Article

Post processing of additively manufactured 316L stainless steel by multi-jet polishing method

Chunjin Wang[*], *Yee Man Loh*, *Chi Fai Cheung*[**], *Xiaoliang Liang*, *Zili Zhang*, *Lai Ting Ho*

State Key Laboratory of Ultra-precision Machining Technology, Department of Industrial and Systems Engineering, The Hong Kong Polytechnic University, Hung Hom, Kowloon, Hong Kong, China

ARTICLE INFO

Article history:
Received 18 December 2022
Accepted 9 January 2023
Available online 11 January 2023

Keywords:
Abrasive water jet
Finishing
Post-processing
Additive manufacturing
Fluid jet polishing
Powder bed fusion

ABSTRACT

Post-process finishing of the additively manufactured (AMed) surfaces is still a critical issue, especially for the AMed surfaces with complex surface geometry, which largely limits the application of additive manufacturing. Hence, this paper presents a multi-jet polishing (MJP) method for post processing of AMed surfaces, utilizing a number of pressurized micro/nanometer abrasive water jets. A group of systematic polishing tests are conducted on 316L stainless steel (SS) prepared by powder bed fusion, to test the polishing performance, as well as the effect of key parameters. Moreover, surface integrity characterization and analysis are also carried out to make full evaluation of the MJP process on AMed 316L SS. The results indicate that MJP is effective for the post processing of AMed 316L SS, to obtain nanometric surface roughness on AMed surfaces, shedding the light on wide application of MJP for AMed complex surfaces.

1. Introduction

Additive manufacturing (AM) technology has gained increasing attention in recent years, and it has become a most promising method for the production of complex components used in various fields, such as optics, aerospace, automotive, electronic, biomedical fields, etc. [1–3], owing to its unique advantages compared to traditional subtractive process, including the ability to produce geometric components with high complexity, the increased speed of part delivery time from design to the market, and the decreased material waste. For example, AM has been successfully adopted to fabricate large size light-weight metallic reflective mirrors through designing complex internal structures [4]. Turbine blades made of Inconel 718 which are typical thin-walled parts with a complex channel inside, can also be fabricated through AM [5]. In the biomedical field, AM has been successfully used to fabricate porous [6,7] and functionally graded structures [8] for load bearing implants, such as hip stem [9].

However, a significant disadvantage arises in the poor surface quality of additively manufactured surface, which has become one of the critical factors limiting the application of AM technology [10,11]. Even though some additively manufactured surface made of polymer materials can achieve a good surface texture, further post-process finishing is still needed for most materials, such as alloys, ceramics, etc. And good surface

* Corresponding author.
** Corresponding author.
E-mail addresses: chunjin.wang@polyu.edu.hk (C. Wang), benny.cheung@polyu.edu.hk (C.F. Cheung).
https://doi.org/10.1016/j.jmrt.2023.01.054

roughness is critical for many high-value-added products, such as artificial implants, engine turbine blades, reflective mirrors, etc. [12–14] Hence, post-process finishing is usually needed. Various kinds of finishing methods have been developed and tested for the post-process finishing of additively manufactured surfaces, including the mechanical type finishing, high energy beam finishing, chemical/electrochemical type finishing, etc.

In mechanical type finishing, the material removal is mainly induced through the application of the abrasive in different way. Sand blasting method has been widely used for the improvement of the additively manufactured external surfaces, especially for the deburring [15]. While shot peening is effective to reduce the surface roughness and improve the mechanical property of additively manufactured surfaces [16]. Wen et al. [17] used the sand blasting method for the finishing of powder bed fusion (PBF) Zn metal, and the surface roughness was reduced from around 10 μm–4.83 μm. Damon et al. [18] demonstrated that the shot peening process not only has the potential to reduce the porosity ratio after PBF, but also can increase the low and high cycle fatigue resistance after shot peening by 20 MPa. As for the internal surface finishing [19] of additively manufactured surfaces, the abrasive flow machining (AFM) shows the best capability to date. Mohammadian et al. [20] presented the AFM of additively manufactured Inconel 625, and the surface roughness was reduced from 7.3 μm to 4.9 μm. The internal surface PBF Inconel 718 was improved from Ra 8–10 μm–1.3 μm after 35 cycles of AFM as reported by Guo et al. [21] In order to speed up the production efficiency, mass finishing method such as vibratory bowl finishing [22], barrel tumbling [23] and drag finishing [24], were also frequently used in industrial field. However, the above-mentioned mechanical type finishing methods have the same problem, which is hard to maintain the surface form and difficult to obtain nanometric surface roughness. Even though some grinding methods such as shape adaptive grinding [25] can implement nanometric surface roughness on additively manufactured surfaces, it is difficult to be used for many kinds of surfaces with complicated geometry.

As for the high energy beam finishing method, the typical one is laser polishing. Lamikiz et al. [26] conducted the laser polishing for the first time on the AISI 420 stainless steel made by PBF method, and the surface roughness was reduced to 1.2–1.3 μm from the initial value of around 7.5 μm. Marimuthu et al. [27] demonstrated the surface roughness reduction from 10.2 μm to 2.4 μm on PBF Ti-6Al-4V samples after laser polishing. Not only the surface roughness improvement, laser polishing can also increase the microhardness and wear resistance of additively manufactured Ti alloy as reported by Ma et al. [28]. However, laser polishing usually suffers from the problem of surface carbonization, oxidation and undesirable phase changes [27,29]. Except for laser polishing, Sankara et al. [30] recently presented the surface quality improvement of PBF maraging steel by large pulsed electron-beam irradiation. But both of the laser polishing and electron-beam irradiation methods can hardly obtain nanometric surface roughness for the application of precision engineering.

For the case of complexed surfaces, especially possessing the components with porous structure, chemical [31] or electrochemical process [32] were usually adopted for the post-process finishing. Zhang et al. [33] investigated the electrochemical polishing of PBF Inconel 718 component, and the surface roughness was improved from 6.05 μm to 3.66 μm only within 5 min Łyczkowska et al. [34] estimated the polishing performance of chemical polishing of additively manufactured scaffolds, and chemical polishing was found to be effective to improve the surface roughness and remove loose powder particles trapped in the porous structure. Crane et al. [35] evaluated a new chemical polishing process called the PUSh™ to reduce the surface roughness of PBF nylon, which is able to reduce the surface roughness from Ra 18 μm–5 μm. Tyagi et al. [36] compared the polishing performance of chemical polishing and electrochemical polishing on additively manufactured 316 steel components. The results showed that electrochemical polishing obtained smoother surface than chemical polishing, while electrochemical polishing has the problem when polishing intricate shapes limited by the accessibility of the counter electrode. The chemical and electrochemical polishing process can implement fast finishing of additively manufactured surface. However, it is difficult for them to maintain the dimensional accuracy of the components.

Except for the above-mentioned methods, some non-traditional methods were also tried by the researchers, such as combined chemical-abrasive flow polishing [20], rotating-vibrating magnetic abrasive polishing method [37], combined ultrasonic cavitation and abrasion method [38], hydrodynamic cavitation abrasive finishing [39] and plasma additive layer manufacture smoothing (PALMS) method [40].

It can be seen that both academia and industry are now working to develop an effective method for the post-process finishing of additively manufactured (AMed) components. A particular challenging issue is to obtain nanometric surface roughness and simultaneously maintain surface form accuracy, which limits the application of additive manufacturing in high value-added precision engineering field. Fluid jet polishing (FJP) method has been widely used in the optical surface polishing field, which can implement nanometric surface roughness together with high form accuracy [41–43]. And different kinds of abrasive water jet methods have also been developed for some other applications [44,45]. But its material removal rate is very slow, leading to limited applications. Qi et al. [46] tried to integrate the assistance of the ultrasonic vibration on the workpiece into FJP to enhance the polishing efficiency, and 44% increasement of the material removal rate was obtained. Beaucamp et al. [47] innovatively developed a novel ultrasonic cavitation assisted FJP system, with the enhancement of the material removal rate up to 380%. The authors recently proposed the multi-jet polishing (MJP) method, which has been proved to be effective to boost the polishing efficiency and maintain high form accuracy [48,49]. Since it can obtain high surface quality as well as optical surfaces, it should also be feasible for the finishing of additively manufactured surfaces. In this paper, a multi-jet post polishing (MJP) method is presented as the post-process finishing method for additively manufactured 316L stainless steel for the first time. The finishing performance of MJP was tested on additively manufactured 316L stainless steel, including the surface roughness, surface form profile, surface composition and microhardness before and after polishing. Moreover, the effect of the key

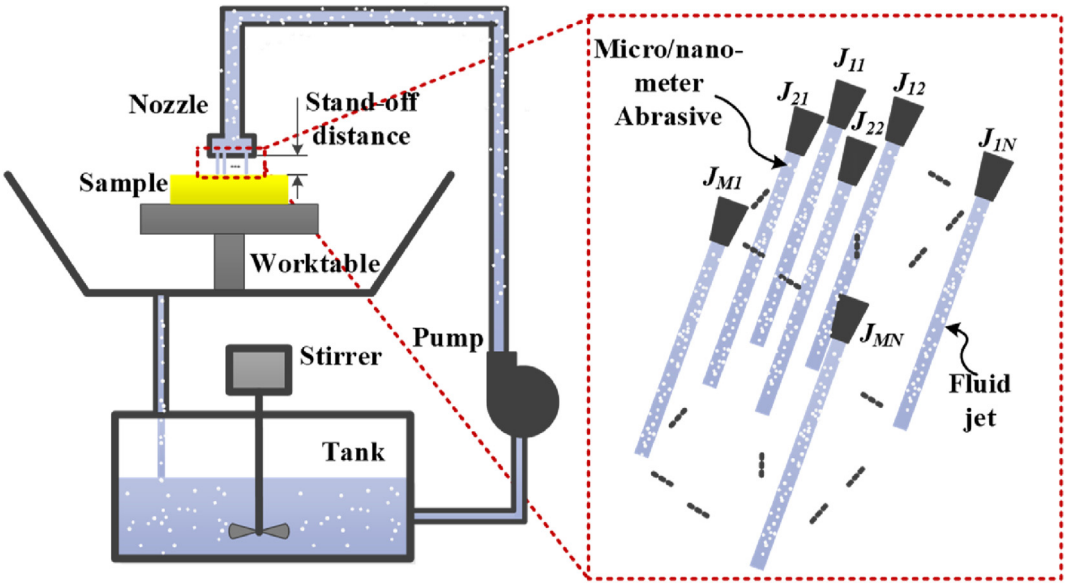

Fig. 1 – Schematic diagram of the multi-jet post polishing (MJP) system.

polishing parameters to the surface roughness was also investigated.

2. Multi-jet post polishing method

Fig. 1 demonstrates the schematic diagram of the MJP method [45]. The polishing slurry is stored in the slurry tank, which can be circulated during the polishing process. During polishing, pressurized slurry with high speed is impinged to the target surface. The micro/nanometer scale abrasive mixed in the slurry can be accelerated by the high-speed water and impinged to the target surface to generate the micro/nano meter scaler material removal, so as to perform the polishing process. A multi-jet nozzle which can generate a number of jets was adopted to boost the polishing efficiency as compared to single jet, while maintaining similar polishing performance with single jet. The material of the abrasive can be silicon carbide (SiC), alumina (Al_2O_3), ceria (CeO_2), silica (SiO_2), etc. And pure water or deionized water is normally used as the base fluid. So, it can be used for the polishing of a wide range of materials.

3. Experimental procedures

3.1. *Specimen preparation*

In this study, a batch of selective laser melted 316L stainless steel (PBF 316L SS) was used for experiments as shown in Fig. 2.

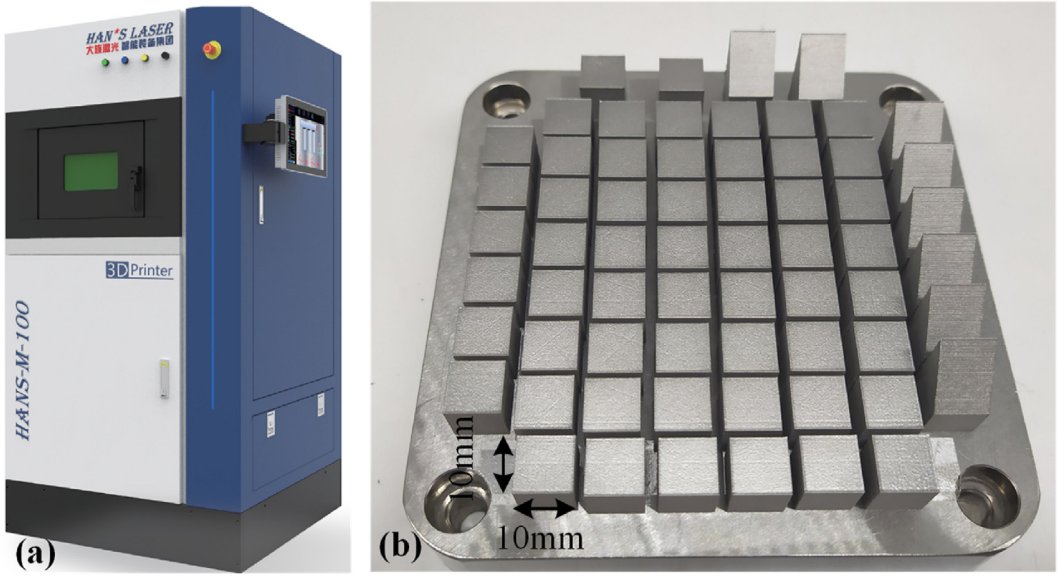

Fig. 2 – Photographs of the (a) PBF equipment and (b) Additive manufactured (AMed) specimens for the experiments.

Table 1 – Conditions for powder bed fusion of 316L stainless steel.

Conditions	Value
Equipment	HANS M100
Material	316L stainless steel
Particle size	0–25 μm
Laser spot diameter	25 μm
Laser power	70 W
Scanning speed	700 mm/s
Hatch distance	0.06 mm
Scan path	Raster path
Layer thickness	20 μm

The PBF conditions are shown in Table 1. The workpieces were cut off from the base using wire electrical discharge machining (WEDM). The workpiece was 10 mm × 10 mm × 10 mm in size.

3.2. Design of the experiments

Fig. 3 demonstrates the experimental set-up, built based on ZEEKO IRP200 polishing machine. All experiments were performed by Zeeko IRP200 Ultra-precision polishing machine as shown in Fig. 3, using #1000 alumina (Al_2O_3) abrasive particles with 10 wt.% concentration. A 7-jet nozzle with 0.5 mm nozzle diameter were used for polishing in this experiment, and the material of the orifice is sapphire. The raster polishing path was adopted to polish the workpiece surface.

To investigate the polishing performance of multi-jet polishing on PBF 316L SS, five groups of mono-factor experiments were designed. Group 1 focused on the difference of polishing performance on the top and side surface under the same polishing conditions. Group 2–5 were conducted to investigate the effect of key parameters of multi-jet polishing, including feed rate, pressure, stand-off-distance and scan interval respectively. Detail conditions are summarized in Table 2.

3.3. Surface and subsurface characterization methods

The surface roughness was measured on a Zygo Nexview white light 3D interferometer. The magnification of the object lens was 40. The lateral and vertical resolutions of the measurement were 208.8 nm and 0.1 nm, respectively. 5 randomly distributed points were measured for each surface. The measurement area for each point was 213.78 μm × 213.78 μm. The arithmetic average surface roughness (Sa) and the surface maximum height (Sz) were utilized to evaluate the surface roughness, which are defined according to ISO25178 standard. The surface roughness was analyzed directly in the software Mx. A nine-order polynomial filter was used, and other settings were the default settings of the software.

The micro-topography of the surface before and after polishing were measured on Alicona Infinite Focus 3D surface measurement system. The surface 3D topography and 2D sectional profile were both analyzed. The size of the measurement area is 1.4305mm × 1.0852 mm. Moreover, an ultra-high resolution field emission scanning electron microscope (FE-SEM, TESCAN MAIA3) was used to analyze the micro/nano surface texture or structure.

The microstructure was obtained by the prepared chemical reagent and then chemically etched for 5 s with corrosive liquids (10 mL HF + 30 mL HNO3). The chemical element analysis of the surface before and after polishing was also analyzed by the energy dispersive x-ray spectroscopy (EDS) integrated in TESCAN MAIA FE-SEM. Meanwhile, an x-ray diffractometer (XRD, Rigaku SmartLab, 9 kW-Advance) was used to conduct the phase change before and after polishing.

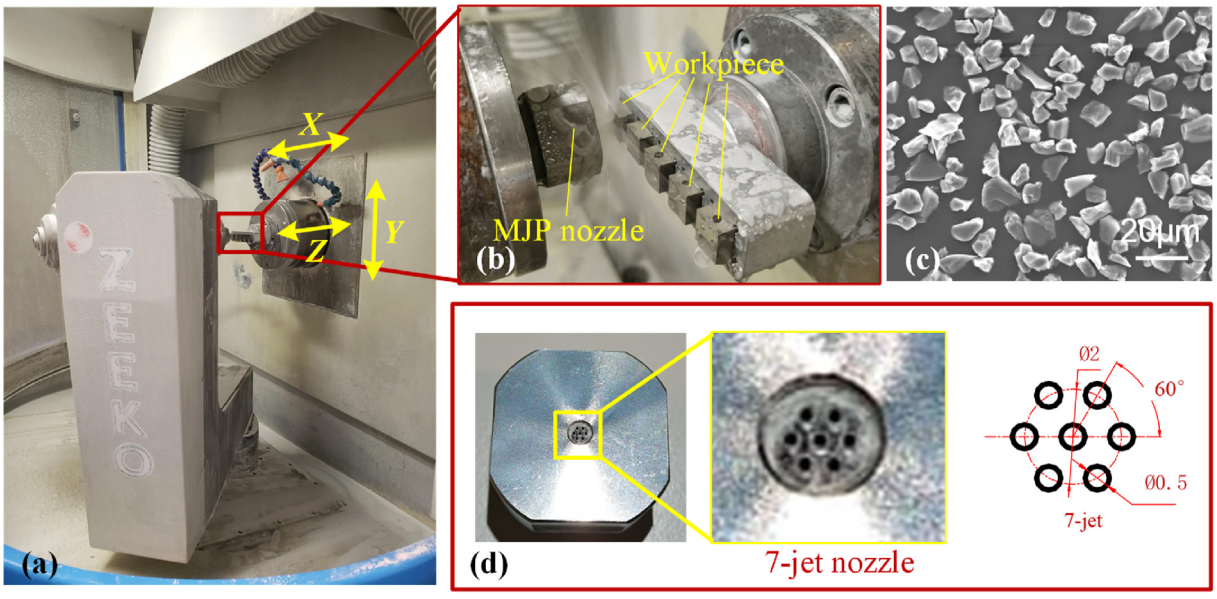

Fig. 3 – Experimental set-up of multi-jet post polishing. (a) Photograph of the experimental set-up on ZEEKO IRP200, (b) Partial enlarged view of the experimental set-up, (c) SEM photograph of the FUJIMI 1000# Alumina abrasive, (d) Photograph and design of the 7-jet nozzle.

Table 2 – Design of the mono-factor experiments.

	Group 1	Group 2	Group 3	Group 4	Group 5
Feed Rate [mm/min]	20	A*	20	20	20
Pressure [bar]	8	8	B*	8	8
Stand-Off-Distance [mm]	5	5	5	C*	5
Scan Interval [mm]	0.2	0.2	0.2	0.2	D*

A* Feed rate: 10, 20, 30, 40, 60, 80 mm/min; B* Slurry pressure: 4, 5, 6, 7, 8, 9, 10 bar.
C* Stand-off-distance: 2.5, 5, 7.5, 10, 12.5, 15 mm; D* Scan interval: 0.1, 0.2, 0.3, 0.4, 0.5, 0.6 mm.

The nanoindentation hardness was tested by NanoTest Vantange, and the test parameters were set as maximum load 50 mN, loading/unloading rate 2.5 mN/s, and dwell time 5s. The top and side surfaces of each sample were tested respectively, and each position was tested at 1 μm, 3 μm, and 5 μm from the surface edge. The nanoindentation hardness test was repeated twice to obtain the gradient nano hardness within 5 μm from the surface on both sides.

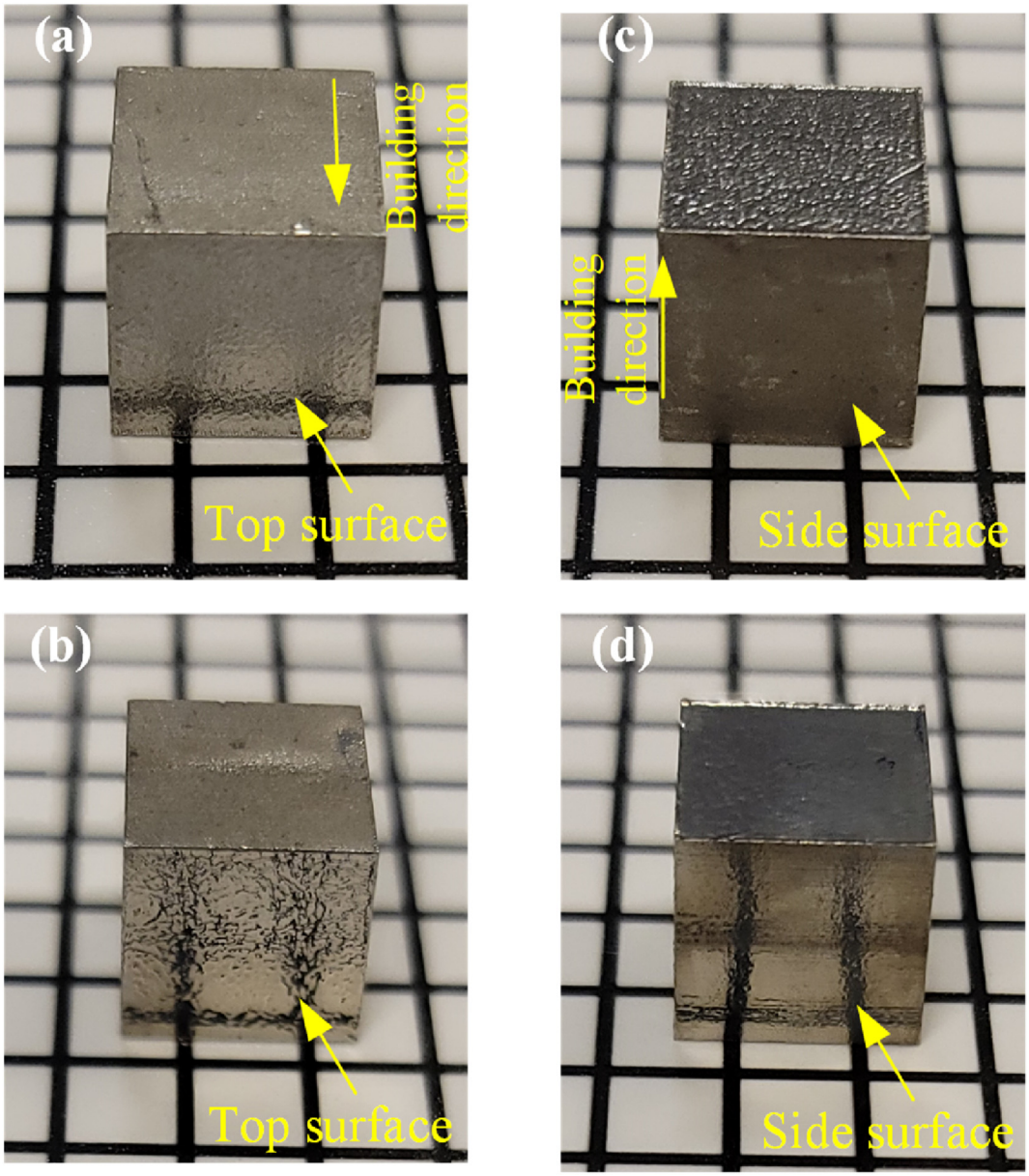

Fig. 4 – Snapshots of the top and side surface before and after MJP. (a) Top surface before MJP, (b) top surface after MJP, (c) side surface before MJP, and (d) side surface after MJP.

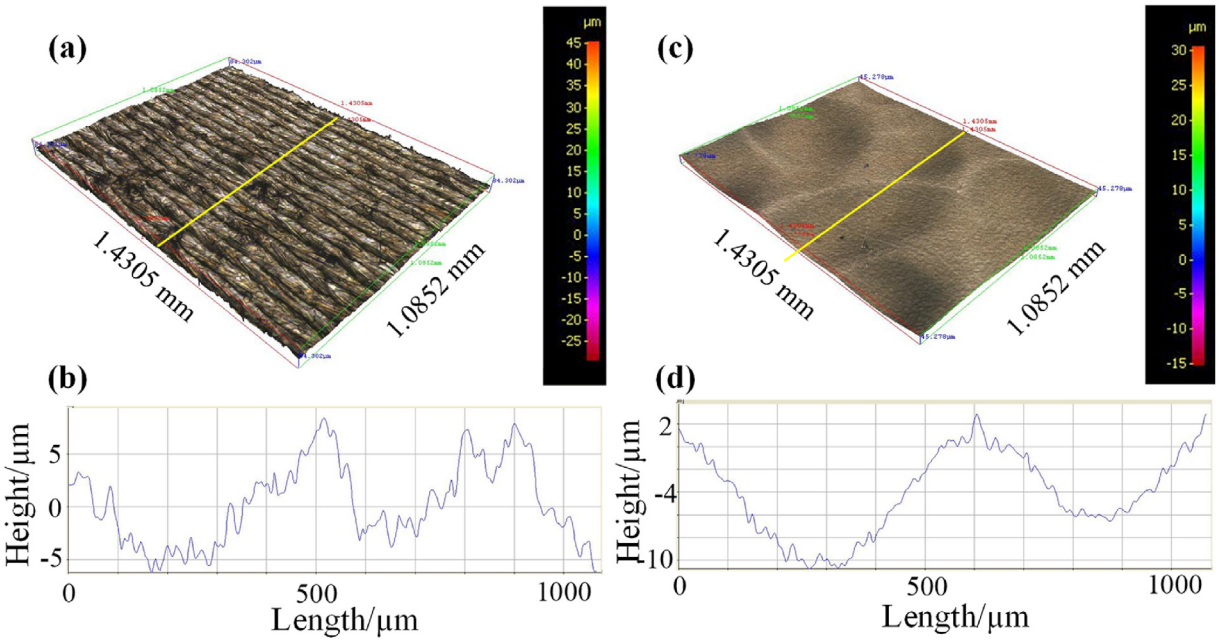

Fig. 5 – Surface topography of the top surfaces before and after polishing measured on Alicona IFM G4. (a) Surface topography of the top surface before polishing. (b) Sectional profile along the yellow line of the top surface before polishing. (c) Surface topography of the top surface after polishing. (d) Sectional profile along the yellow line of the top surface after polishing (The sectional profile corresponds to the yellow line).

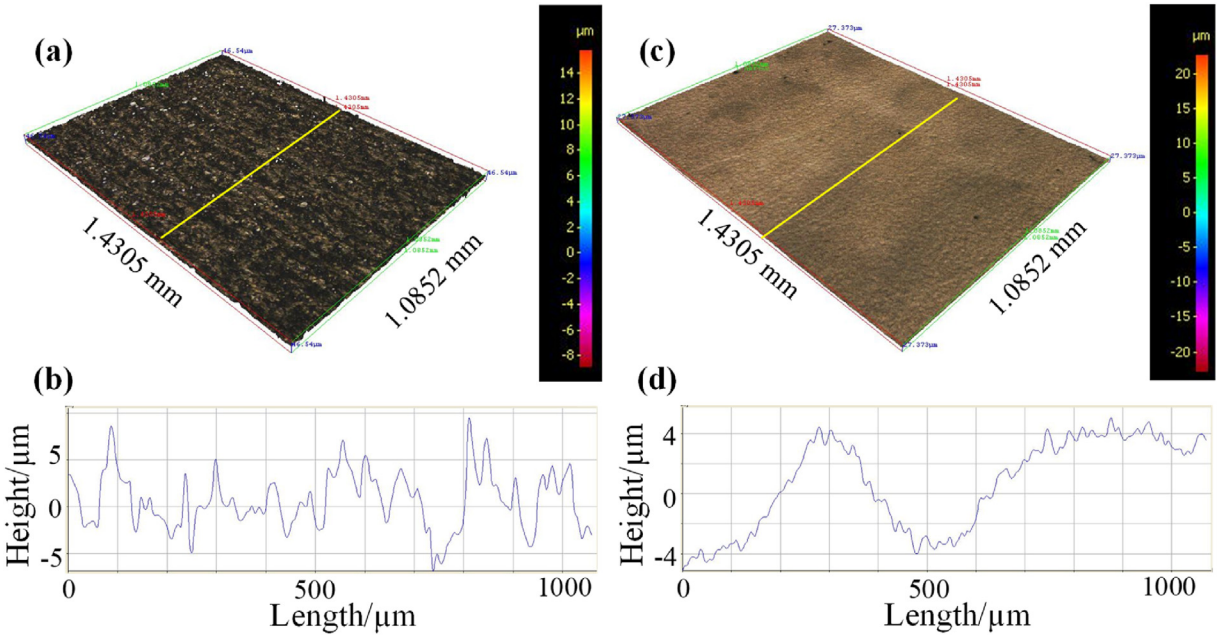

Fig. 6 – Surface topography of the side surface before and after polishing measured on Alicona IFM G4. (a) Surface topography of the side surface before polishing. (b) Sectional profile along the yellow line of the side surface before polishing. (c) Surface topography of the side surface after polishing. (d) Sectional profile along the yellow line of the side surface after polishing (The sectional profile corresponds to the yellow line).

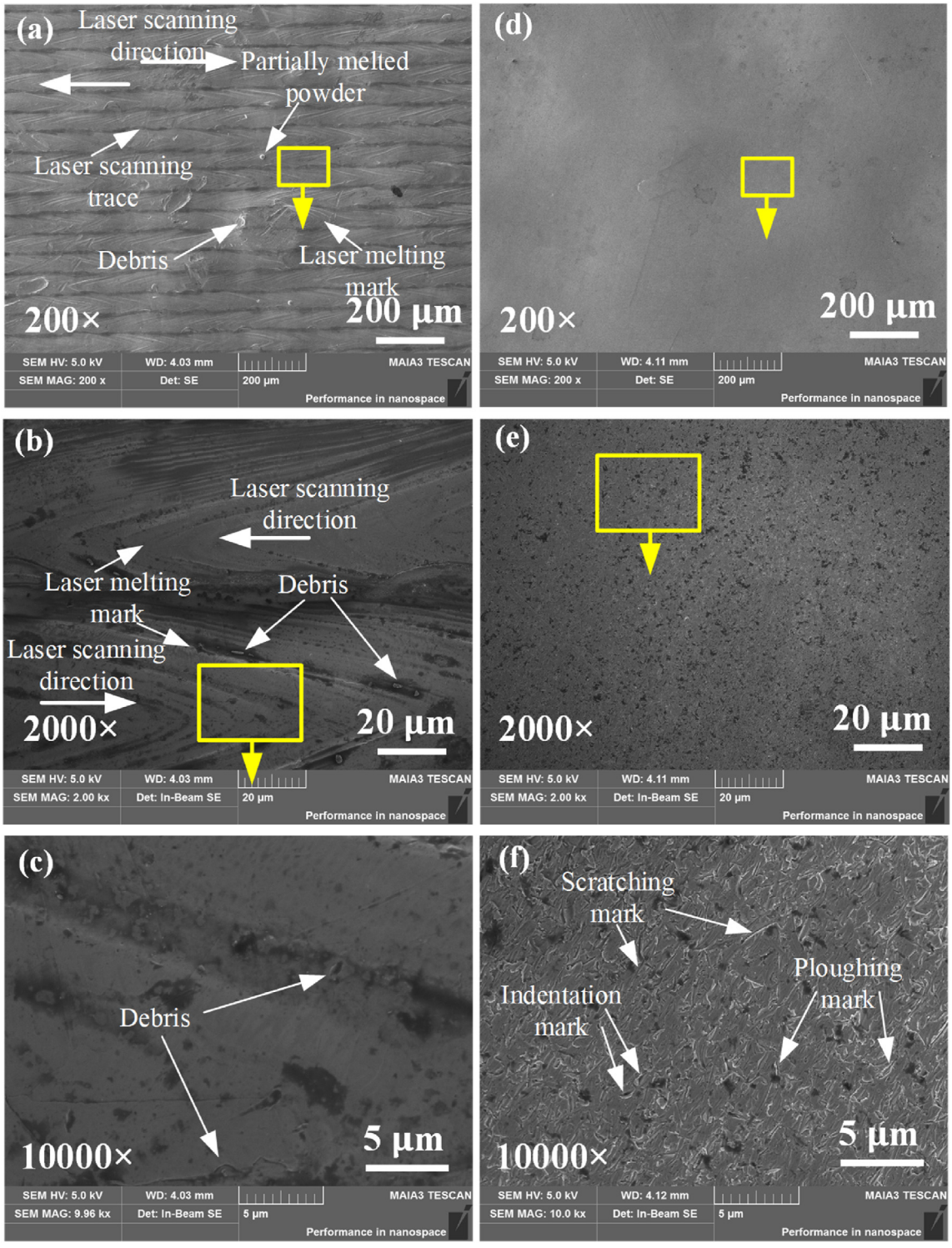

Fig. 7 – SEM photographs of the top surfaces before and after polishing under different magnifications. Surface topography before polishing under the magnification of (a) 200 × , (b) 2000 × , and (c) 10,000 × . Surface topography after polishing under the magnification of (d) 200 × , (e) 2000 × , and (f) 10,000 × .

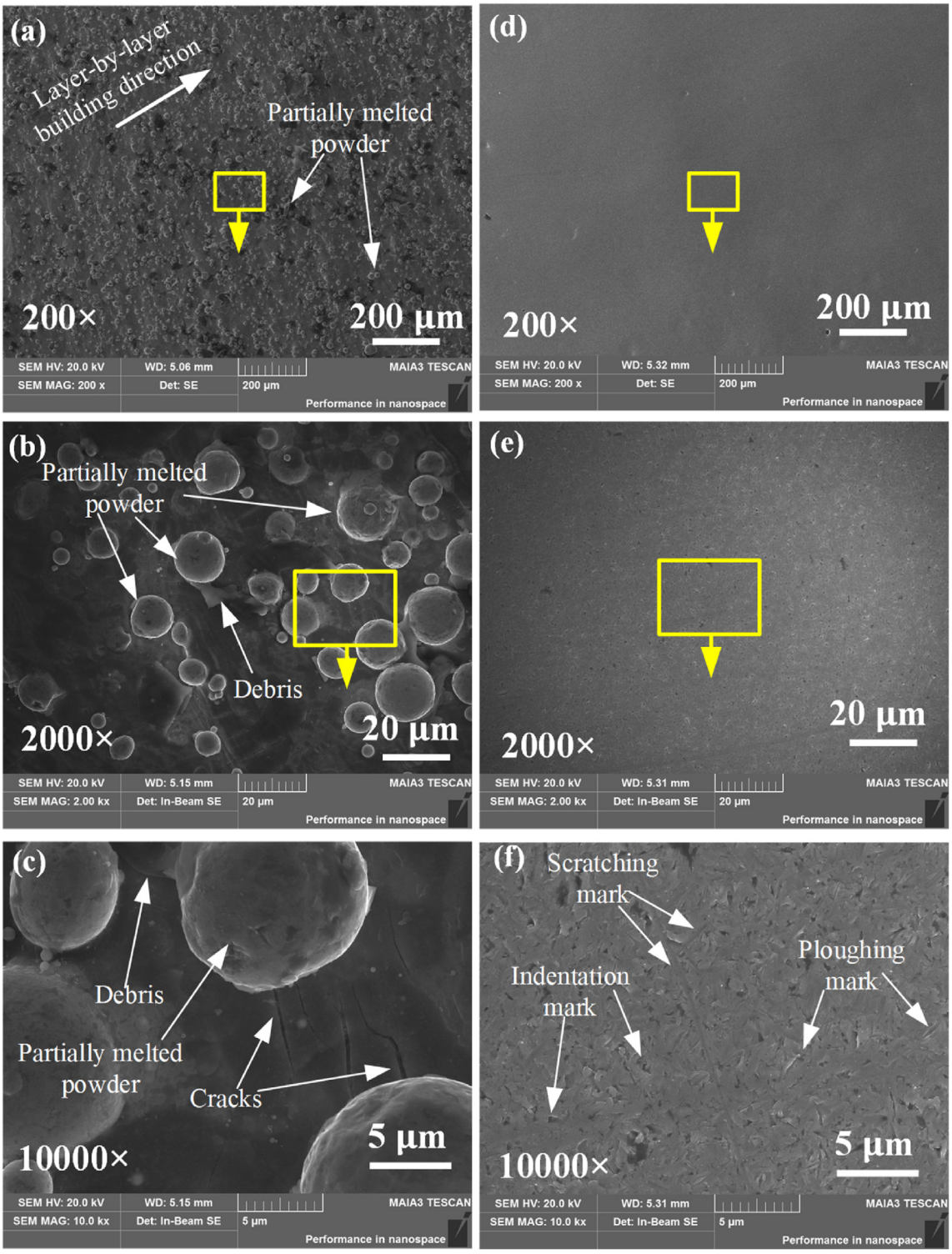

Fig. 8 – SEM photographs of the side surfaces before and after polishing. Surface topography before polishing under the magnification of (a) 200 × , (b) 2000 × , and (c) 10,000 × . Surface topography after polishing under the magnification of (d) 200 × , (e) 2000 × , and (f) 10,000 × .

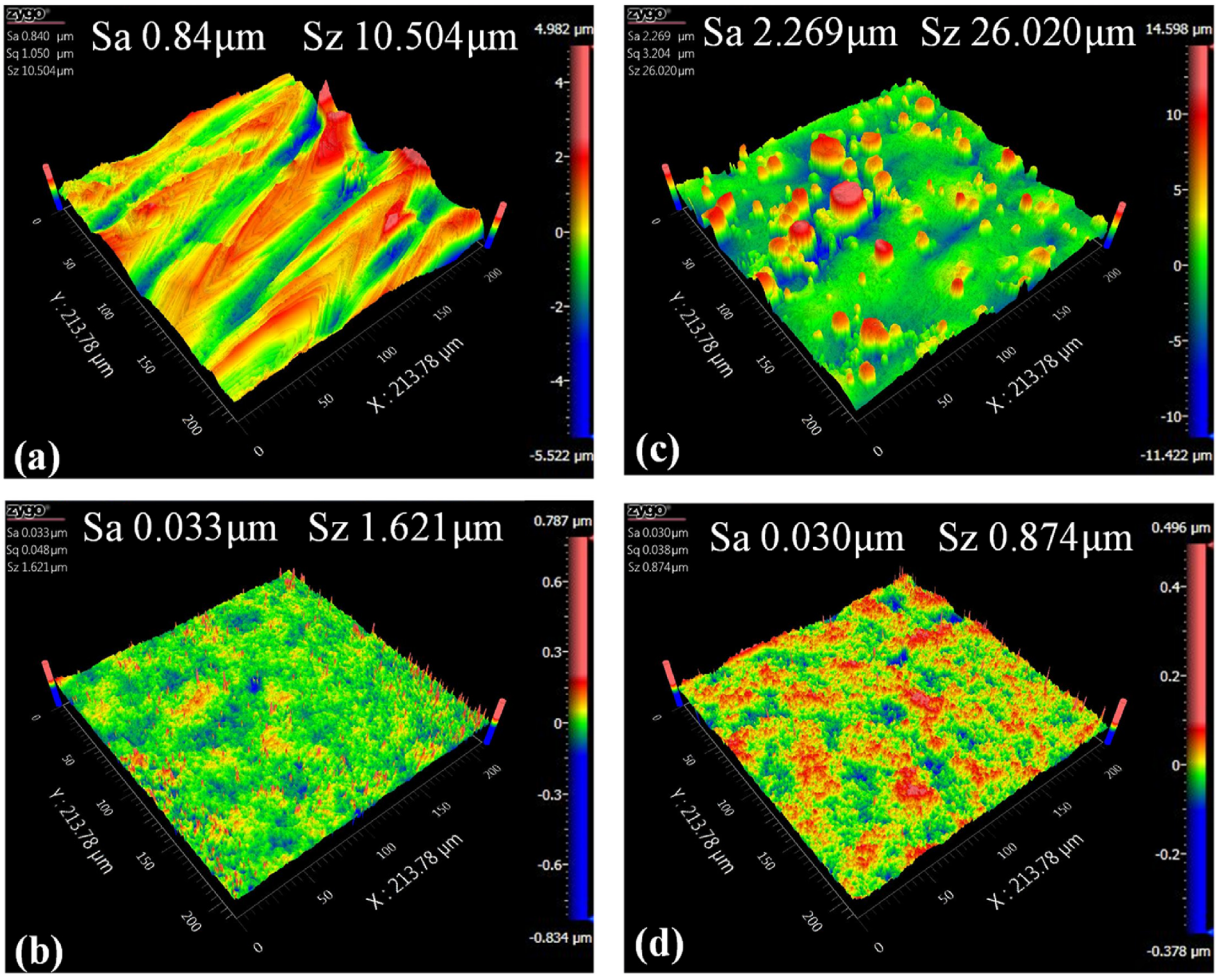

Fig. 9 – Surface roughness analysis results. Surface roughness contour of the top surface (a) before polishing and (b) after polishing. Surface roughness contour of the side surface (c) before polishing and (d) after polishing.

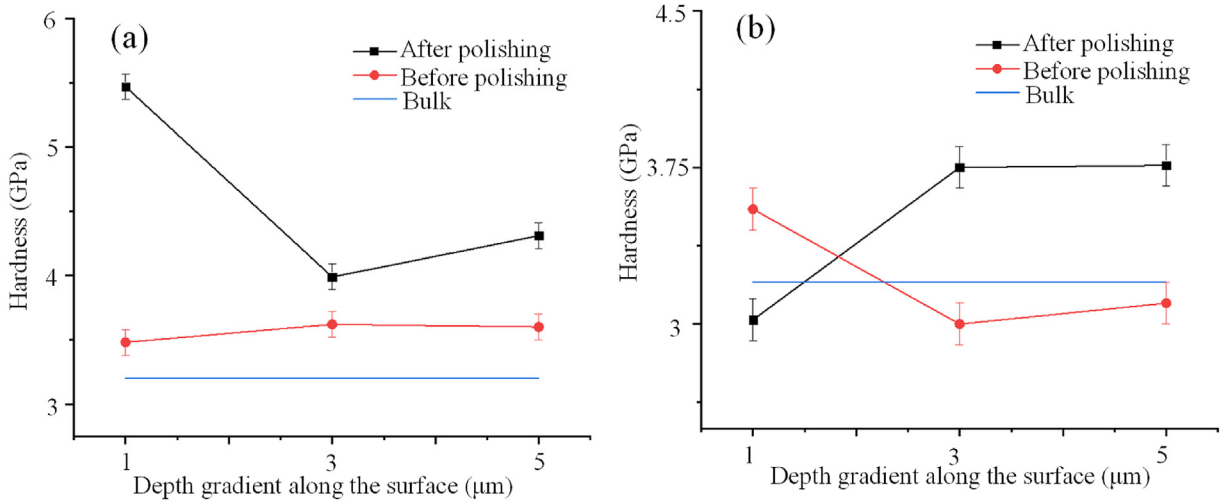

Fig. 10 – Subsurface micro-hardness results at different depths before and after polishing. (a) Top surface, and (b) side surface.

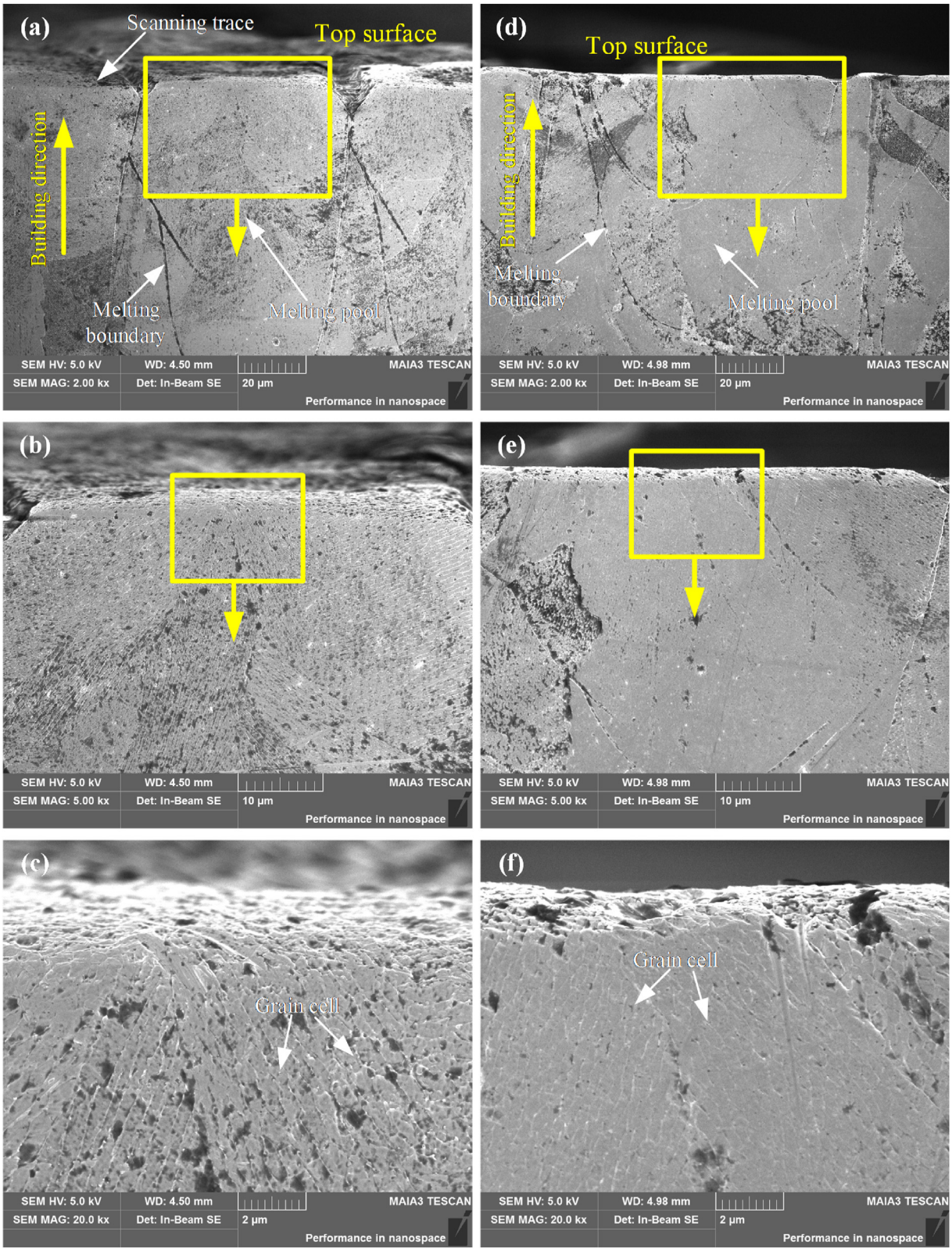

Fig. 11 – SEM photographs of the subsurface layer of the top surface before and after polishing. Subsurface microstructure of the top surface before polishing under different magnifications of (a) 2000 × , (b) 5000 × and (c) 20,000 × . Subsurface microstructure of the top surface after polishing under different magnifications of (d) 2000 × , (e) 5000 × and (f) 20,000 × .

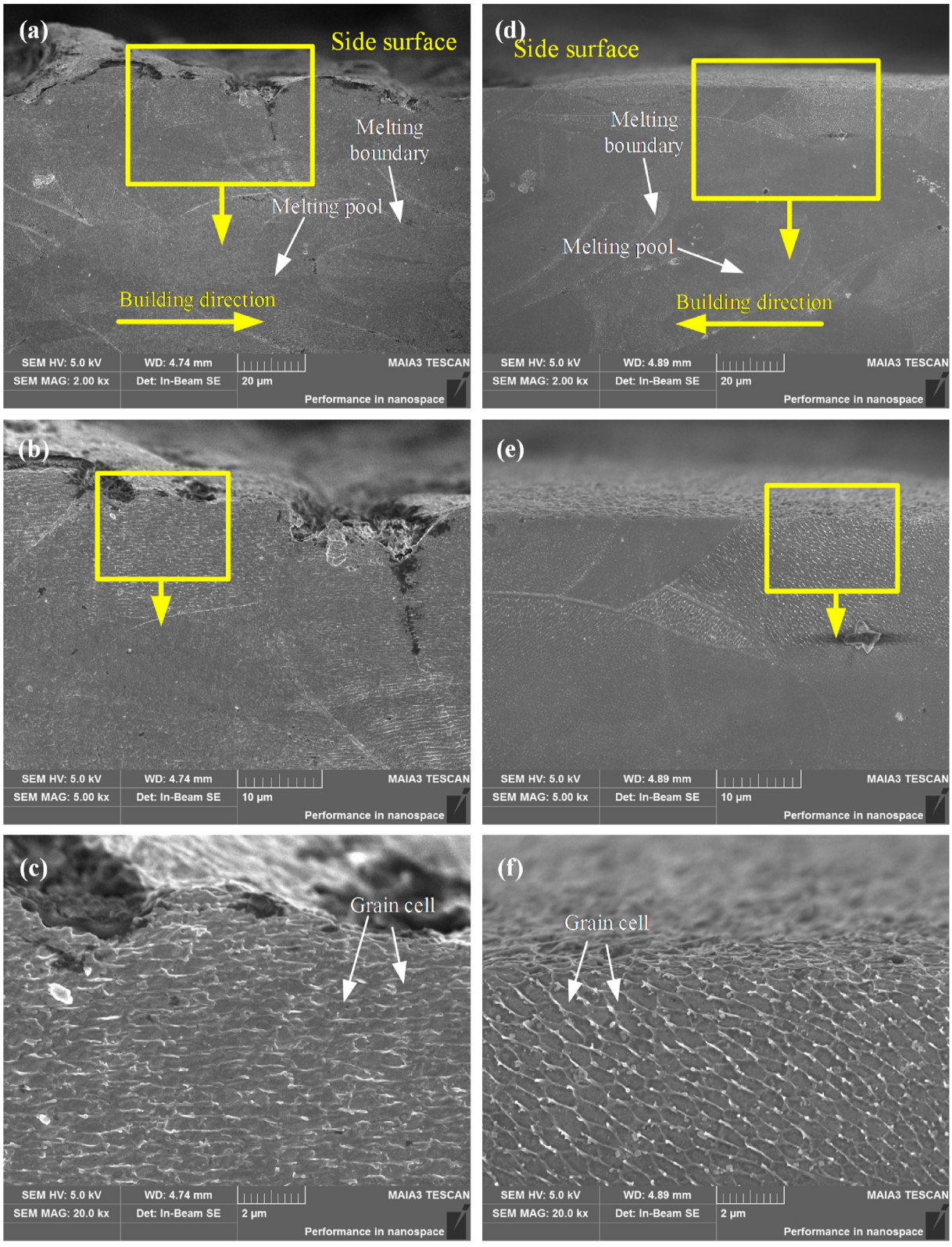

Fig. 12 – SEM photographs of the subsurface layer of the side surface before and after polishing. Subsurface microstructure of the side surface before polishing under different magnifications of (a) 2000 × , (b) 5000 × and (c) 20,000 × . Subsurface microstructure of the side surface after polishing under different magnifications of (d) 2000 × , (e) 5000 × and (f) 20,000 × .

4. Results and discussions

4.1. *Analysis of surface topography and surface roughness*

Fig. 4 shows the snapshots of the workpiece before and after polishing. The top and side surfaces were largely smoothened to obtain a much shiny surface with mirror-like property. In order to observe the micro-topography of the surface, the surfaces before and after polishing were observed on Alicona InfiniteFocus 3D surface measurement system, and the results of the top surface and side surface are demonstrated in Figs. 5 and 6, respectively. As shown in Fig. 5(a), obvious laser melting marks along the scanning direction of laser during PBF can be observed on the surface before polishing. The interval between the laser melting mark is exactly the same with the path scan interval (hatch distance) as shown in Table 1. After MJP, the laser melting marks were successfully eliminated, and the surface was smoothened as shown in Fig. 5(c). As for the side surface, many partially melted powders can be observed before polishing showed in Fig. 6(a), which are induced by the unmelted powders remaining in the laser beam and powder bed boundary zone during the PBF process. In addition, layer-by-layer building marks can also be observed in the side surface. After MJP, both the partially melted powders and layer-by-layer building marks were successfully removed as shown in Fig. 6(c). Even though the PBF surface after MJP can be smoothened, such as removing debris, laser melting marks, and layer-by-layer building marks, millimeter scale waviness form error is left after polishing. This should be induced by the initial surface form error of the surface after PBF and cannot be corrected by MJP.

In order to analyze the microscale surface topography, both the top surface and side surface before and after polishing were also measured on a MAIA TESCAN FE-SEM. The surface topography of them were clearly demonstrated at three different magnifications of 200, 2000 and 10,000. Figs. 7 and 8 shows the top and side surfaces before and after polishing under different magnifications, respectively. Except for the laser melting marks, some debris can also be clearly observed on the top surface before polishing showed in Fig. 7(a)~(c). As for the side surface before polishing, the partially melted powders, as well as the debris and cracks can all be clearly seen on the surface before polishing as shown in Fig. 8(a)~(c). After MJP, the laser melting marks, partially melted powders, debris and cracks are all eliminated both on the top and side surfaces as presented in Fig. 7(d)~(f) and Fig. 8(d)~(f). It reveals that MJP can successfully smoothen the PBF 316L SS. Only the micrometer scale erosion marks were left on the surface as shown in Figs. 7(f) and Fig. 8(f), which are caused by the impinging of the alumina abrasive on the surface. The erosion mark in fluid jet polishing includes abrasive indentation, ploughing, and scratching [50].

The surface roughness of the top and side surface before and after polishing were also measured on Zygo Nexview white light interferometer as shown in Fig. 9. The surface roughness in Sa of the top surface was reduced from 0.84 um to 0.033 μm, and Sz was reduced from 10.504 μm to 1.621 μm. The surface roughness reduction of the top surface in Sa can reach 96.07%. While the surface roughness in Sa of the side surface was reduced from 2.269 μm to 0.03 μm, and Sz was reduced from 26.02 μm to 0.874 μm. The surface roughness reduction of the side surface in Sa can reach 98.68%. It indicates that the MJP is effective to largely reduce the surface roughness of the PBF 316L SS. The surface roughness of the side surface was much larger than the top surface, which are caused by the partially melted powders.

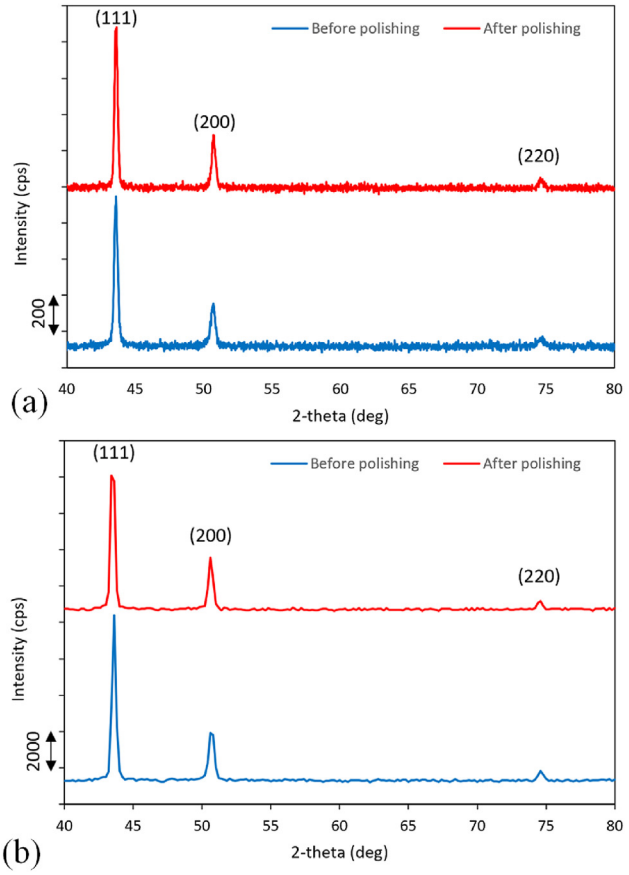

Fig. 13 – XRD analysis of the surface before and after polishing. (a) Top surface, and (b) side surface.

4.2. *Analysis of material hardness and microstructure*

The microhardness of the top and side surface before and after polishing were also measured to analyze effect of the polishing process to the material mechanical property. Fig. 10 shows the microhardness measurement result of the top and side surface before and after polishing. It is noted that the microhardness of the top surface became larger after MJP. When the depth is 1 μm, the microhardness was increased from 3.5 GPa to 5.5 Gpa as shown in Fig. 10(a). And the increasement becomes smaller with the increasing of the depth. The reason for the hardness increasement is that the material removal during MJP is induced the impinging of the micro-meter scale abrasive, which is similar to the blasting process or shot peening process. And it has been reported that shot peening and sand blasting can increase the hardness of

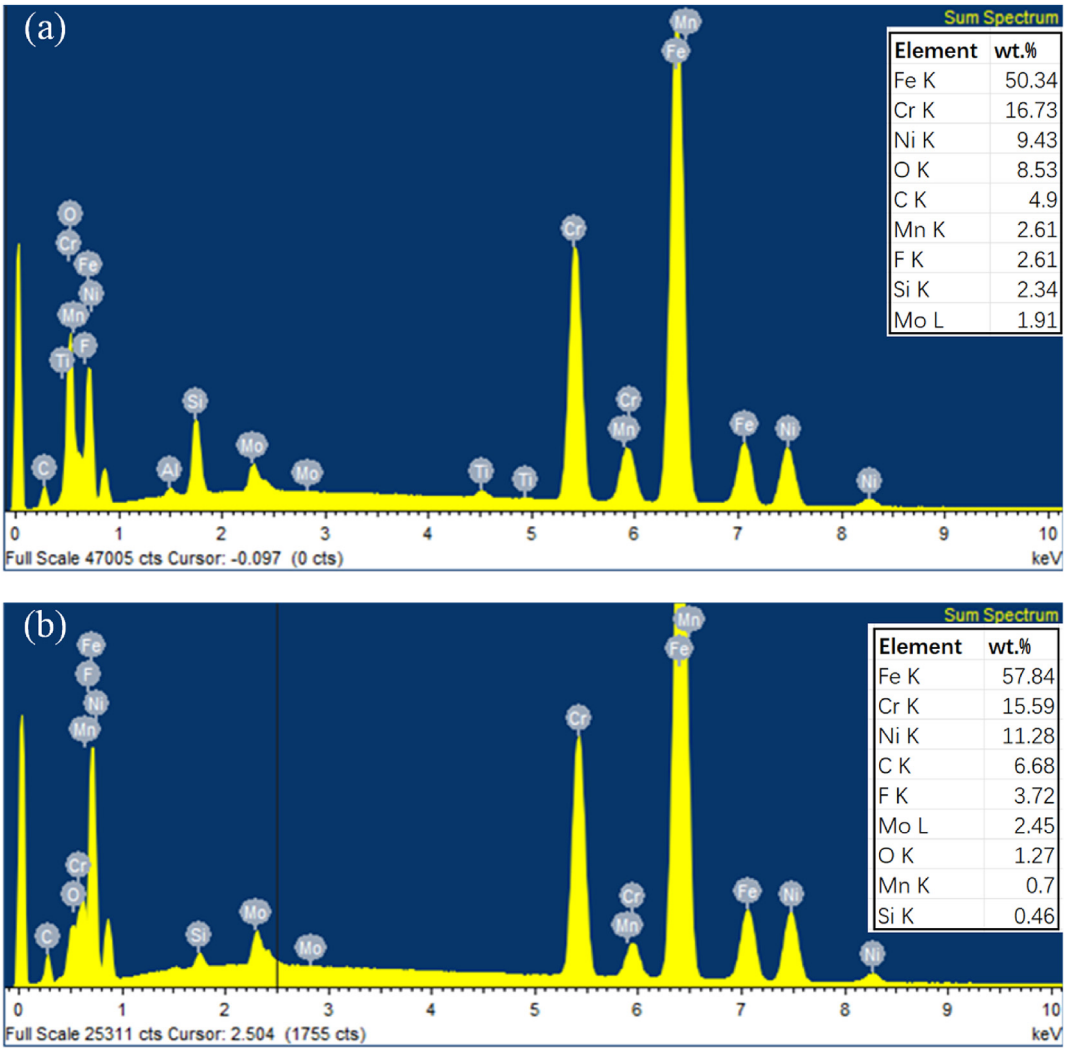

Fig. 14 – Composition analysis of the top surface (a) before and (b) after polishing.

the additively manufactured alloy surface [51,52]. Considering that the abrasive in MJP is in micrometer scale, while the size of particle used in shot peening and sand blasting is much larger. Hence, the impinging force of each particle in MJP is smaller than shot peening and sand blasting, leading to the thinner hardness enhancement layer. In shot peening or sand blasting, the surface is deformed under the indentation of the particle. Nevertheless, except for the indentation, ploughing and scratching process are also occurred under the effect of the fluid, which is the main reason to obtain nanometric surface roughness. As for the side surface, the microhardness increasement is not obvious as shown in Fig. 10(b), because this surface is interrupted by the laser melting layer, which is harmful for hardness enhancement.

In order to analyze the surface microstructure of PBF 316L SS before and after polishing, SEM photographs on the sectional surface were taken as shown in Figs. 11 and 12. The melting pool and boundaries can be clearly observed on the section surface, as well as the scanning trace showed in Fig. 11(a). The width of the melting pool is around 40 μm. And the interval of each melting layer is around 20 μm showed in Fig. 12(a), corresponding to the layer thickness. Micrometer scale grain cells can also be observed clearly observed, as demonstrated in the bottom parts of Figs. 11(c) and Fig. 12(c). The size of the grain cell is about ~0.5 μm–1.5 μm, which agrees well with previous studies [24,53,54]. The results also indicate that MJP is effective to remove the surface debris, laser melting marks, and defects. Moreover, no obvious change of the microstructure can be observed between the section surface before and after polishing.

4.3. *Analyze of material phase and composition before and after polishing*

XRD analysis was also conducted to investigate if there is phase change after MJP. The XRD comparison of both the top and side surface before and after polishing were shown in Fig. 13. The peak positions and values are quite similar to the PBF 316L stainless steel as reported by Kaynak and Kitay [24]. It is noted that the XRD curve of the surface after polishing are almost the same with the result before polishing, indicating no obvious phase change after MJP. Except that there exists

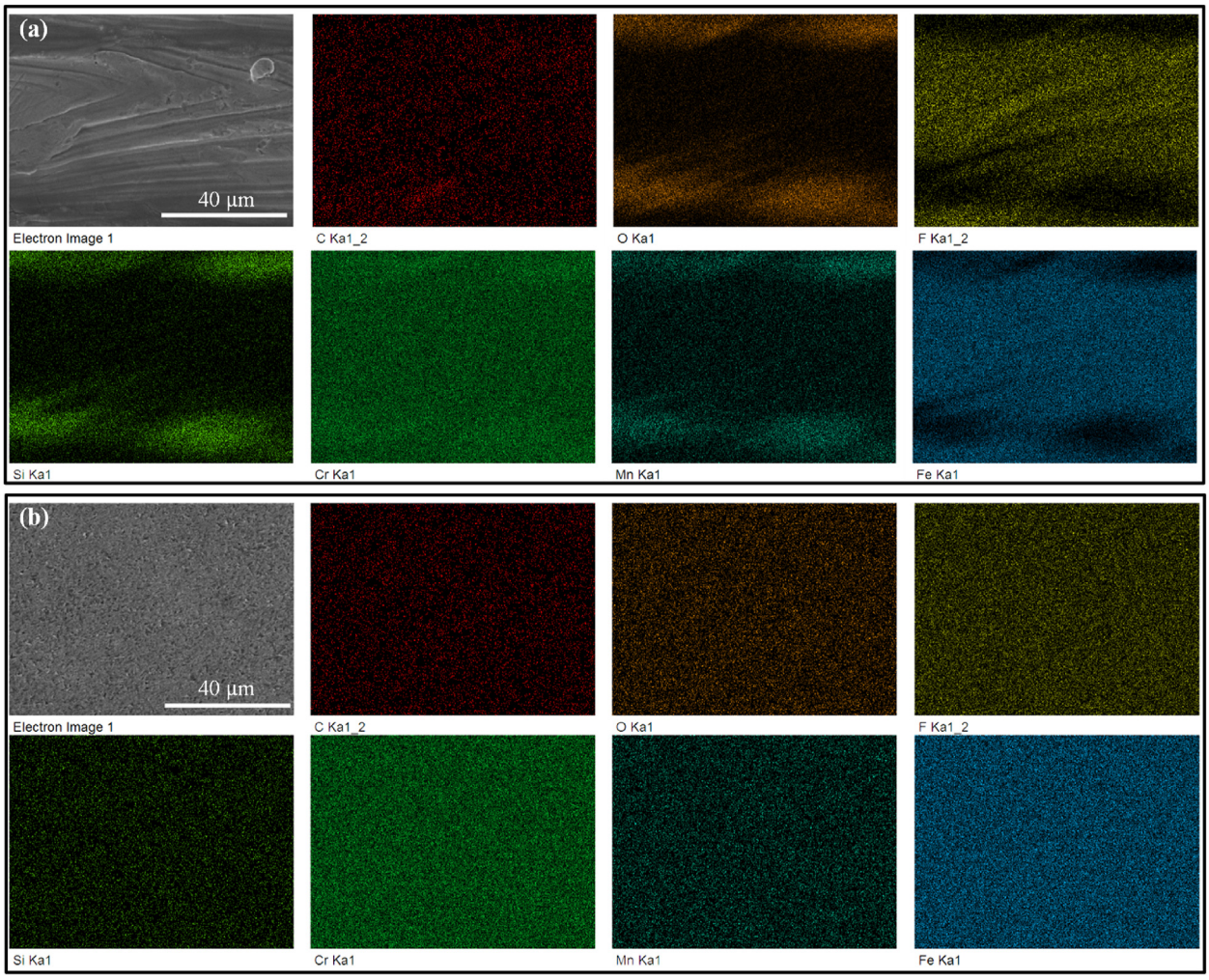

Fig. 15 – EDS results of the element distribution (a) before and (b) after MJP (Only the elements with the weight percentage larger than 0.4% are demonstrated here).

tiny difference on the peak value, which is induced by the different surface roughness.

To further investigate the chemical composition of the surface before and after MJP, EDS analysis was also conducted. The analysis was conducted on the top surface only, since the chemical composition on the top and side surface are the same. Fig. 14 shows the analysis results of the composition of the top surface before and after polishing. No obvious change can be found on the surface, suggesting that MJP has no effect on the chemical composition of the PBF 316L SS. In addition, it is noted that the percentage of the Oxygen element is reduced after polishing. Because there exists oxidization during the high temperature laser melting process, generating oxide layer on the surface. The oxide layer was removed after polishing, resulting in the reduction of the oxide element. Moreover, it can be seen that the distributions of some elements are not evenly distributed on the surface induced by the laser scanning trace as shown in Fig. 15 (a). Whereas these elements turned into evenly distributed after MJP, induced by the smoothen of the surface (Fig. 15(b)).

4.4. *Effect analysis of key parameters*

Except for the above analysis of the surface integrity, the effect of some key parameters is also conducted in this paper, including fluid pressure, stand-off distance, scan interval and feed rate. The top surface was used as the test surface in this study.

Fluid pressure is one of the key factors in fluid jet polishing process, 6 pressure levels were tested in this experiment. The average value of the surface roughness of the top surface used for this experiment is Sa 0.774 μm. Within this pressure range, the general trend is that larger fluid pressure results in lower surface roughness as shown in Fig. 16(a). When the fluid pressure is smaller than 6 bar, the surface roughness is all higher than 80 nm. While the surface roughness decreases dramatically when the fluid pressure is 7 bar, which are all around 40 nm. In fluid jet polishing, high fluid pressure can obtain higher material removal rate [55]. When the fluid pressure is lower than 6 bar, the material removal is not enough to eliminate the surface defects, leading to the high

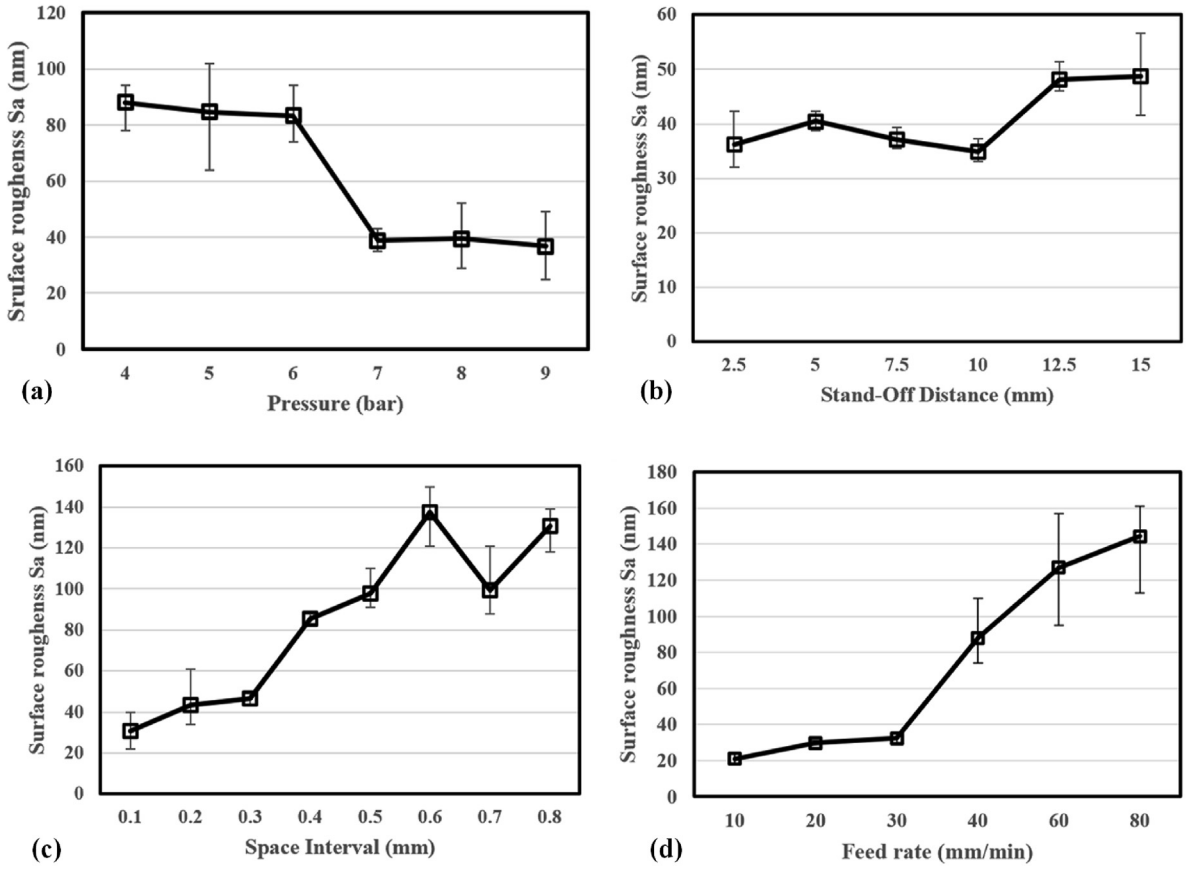

Fig. 16 – Effect analysis on four key parameters in MJP to the surface roughness. (a) Fluid pressure, (b)Stand-off distance, (c) scan interval, and (d) feed rate.

surface roughness. Hence, the fluid pressure in MJP of PBF 316L SS should be larger than 6 bar to obtain better surface roughness.

Fig. 16(b) shows that the polished surface roughness varies with the stand-off distance. It is noticed that the surface roughness has no obvious relationship to the stand-off distance within normal working range as reported in previous publication [56]. Because the effect of the stand-off distance to the material removal rate is not significant. When the stand-off distance is in the range of 2.5 mm–10 mm, the surface roughness is around 40 nm. When the stand-off distance is larger than 10 mm, the material removal rate becomes lower, induced by the reduced energy of the jet.

Scan interval and feed rate are key parameters in fluid jet polishing which also determines the polishing time of the process. The effect of scan interval and feed rate on MJP additive manufactured (AMed) 316L SS are shown in Fig. 16(c) and (d), respectively. Both two parameters show a positive relationship with surface roughness, a larger scan interval and higher feed rate would result in higher surface roughness value. In Fig. 16(c), the change in scan interval resulted in a relatively constant increase in surface roughness, 0.1 mm interval shows the best performance after polishing of 27 nm. Because when the scan interval is 0.1 mm, which is the minimum one, it corresponds to the longest polishing time. Hence, the surface defects can be thoroughly removed, giving rise to the lowest surface roughness. On the other hand, increase in feed rate shows different trends in 10–30 mm/min and 40–80 mm/min as indicated in Fig. 16(d). A sudden raise has occurred at 40 mm/min, which reveals that 40 mm/min may not have allowed sufficient time for abrasive particles to perform certain extent of material erosion. Hence, the feed rate smaller than 40 mm/min is recommended in MJP of PBF 316L SS in this study. However, with a smaller interval and lower feed rate, the scanning path for polishing would be longer and more time consuming, a balance and trade-off between processing time and polishing performance is needed.

4.5. *Discussion on the material removal mechanism in MJP of PBF surface*

In MJP, a number of fluid jet arrays polish the surface simultaneously, and each jet has almost the same energy, leading to similar material removal mechanism. Fig. 17(a) presents the simulation result of the velocity distribution during the single fluid jet polishing (FJP) process. Detail simulation procure and modelling information can be found in [55]. The diameter of the orifice is 0.5 mm. The fluid pressure is 8 bar. The stand-off distance is 5 mm. It is noted that the velocity is close to 0 at the

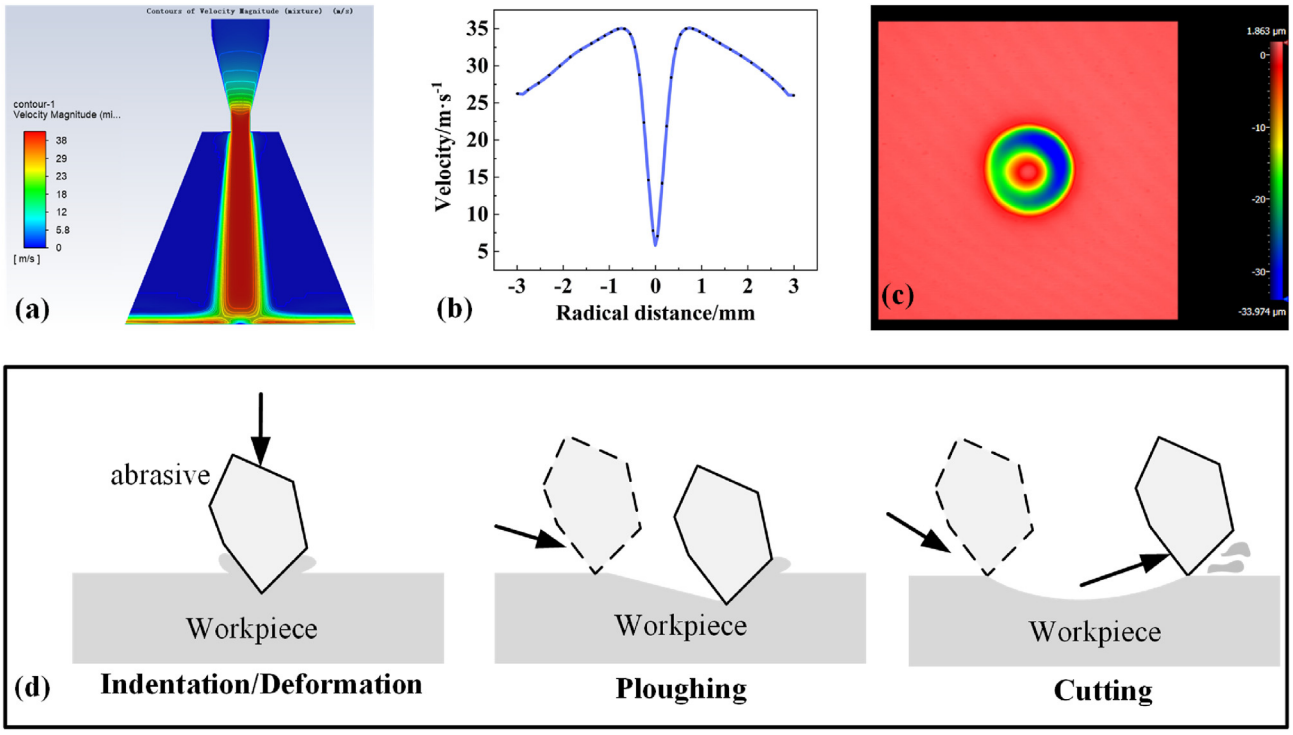

Fig. 17 – Material removal mechanism of fluid jet polishing. (a) Simulated velocity distribution of the fluid during polishing (Diameter of the orifice is 0.5 mm; Fluid pressure is 8 bar; Stand-off distance is 5 mm) (b) Sectional distribution of the fluid velocity on the target surface. (c) Tool influence function of single jet polishing when dwell time is 3 min. (d) Three modes of the erosion behavior of the abrasive.

center of the impinging region. The sectional profile of the velocity distribution along the target surface has also been extracted as shown in Fig. 17(b), it is observed that the velocity in the center is the smallest, which is almost close to zero, and turns to the largest first and decrease gradually from the center to external region. Fig. 17(c) shows the measured tool influence function (TIF) of the single fluid jet on PBF 316L SS. In order to extract the TIF accurately, micro-milling was conducted before the TIF generation experiment to obtain a plane surface. It is noted that the shape of the TIF is like a 'W' shape, which means that the material removal at the center region is the smallest. The cutting velocity becomes larger first and then decreases gradually from the center to the edge. It is different with the high-pressure abrasive water jet machining [57], whose TIF shapes are 'U' shape or gaussian-like shape [58]. Because in FJP, the deformation or indentation has much less contribution to the material removal, induced by the relatively small energy of each abrasive. The material removal in FJP is mainly induced by the ploughing and cutting removal mode as shown in Fig. 17(d).

The material removal mechanism of single fluid jet polishing is also suitable for MJP, since MJP is just a combination of an array of fluid jets. Fig. 18(a) shows the TIF of MJP under the same conditions of the result in Fig. 17. Seven 'W' shape TIFs can be clearly seen on the TIF of MJP, except for some shape deformation affected by the jet interference. The material removal of each jet is quite similar. The material removal mechanism of MJP of PBF 316L SS on top and side surfaces are shown in Fig. 18(b) and (c), respectively. On the top surface, there are defects such as laser scanning trace, partially melted powder, and debris. After MJP, these defects are all eliminated induced by the erosion of the alumina abrasive as shown in Fig. 18(b), including the obvious laser scanning trace and laser melting mark, which can be proved by the results in Fig. 7. Nevertheless, the millimeter scale waviness error existed on the as built (before finishing) surface cannot be smoothened to be a flat surface, indicated from Fig. 5. It infers that MJP can maintain the surface form well, while it cannot improve the surface form. This is the reason why FJP can be used for the polishing functional structured surfaces [42]. As for the side surface, there are many partially melted powders on this surface, as well as some debris and cracks. After MJP, almost all these defects can be removed as shown in Fig. 18(c), which can be proved by the results in Fig. 8. Similarly, the millimeter scale waviness error cannot be smoothened to be a flat surface, indicated from Fig. 6. Hence, MJP is effective to remove the surface defects and improve the surface roughness of the PBF 316L SS. Just like other post-processing methods (i.e. laser polishing, chemical polishing, abrasive flow finishing, etc.), MJP cannot improve the form accuracy of the as-built surface.

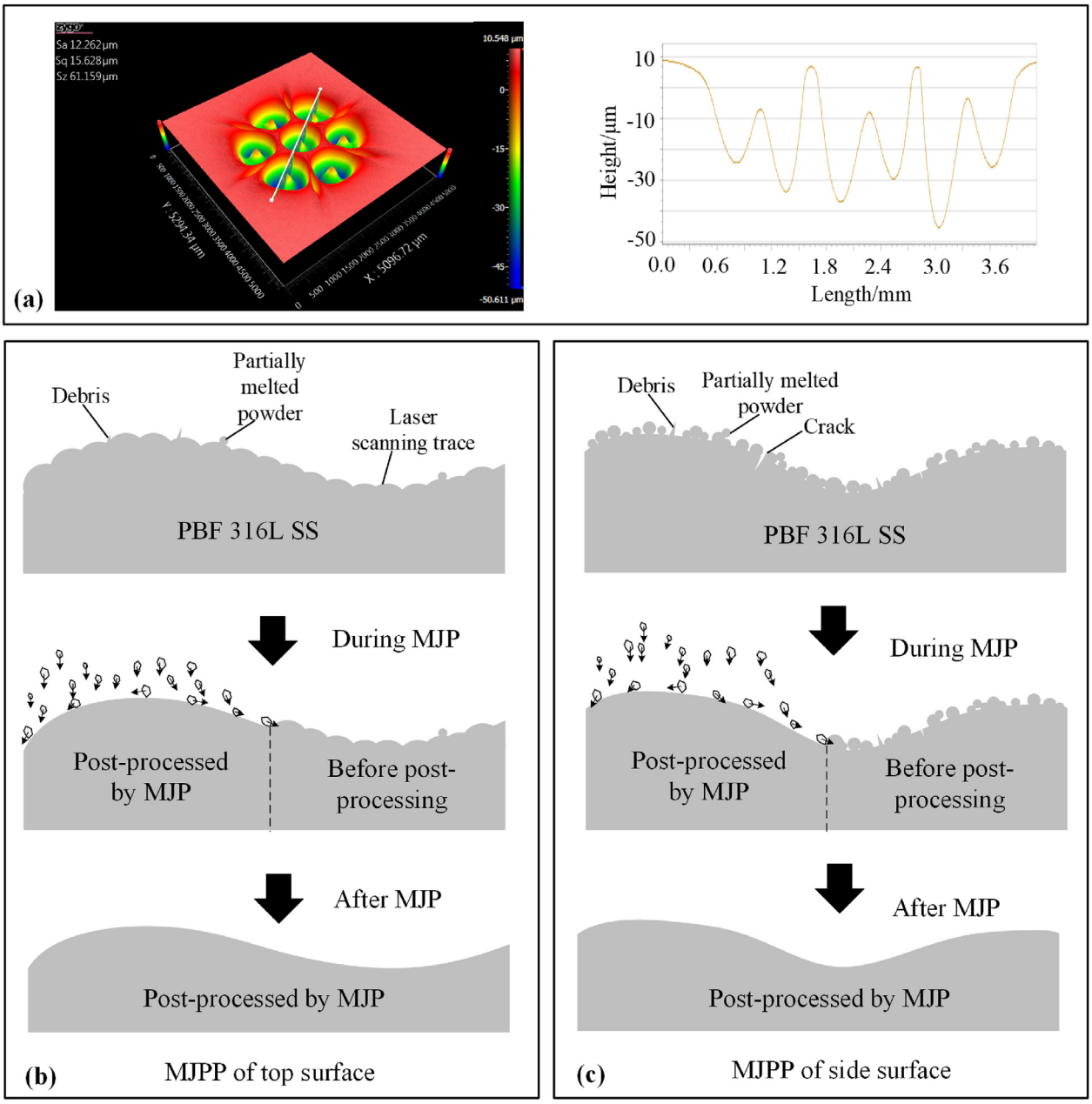

Fig. 18 – Material removal mechanism of MJP on PBF 316L SS. (a) Tool influence function of MJP including 3D contour and 2D sectional profile. (b) Material removal mechanism of MJP the top surface of PBF 316L SS. (c) Material removal mechanism of MJP the side surface of PBF 316L SS. Considering that there exists surface form error before polishing, waviness form is shown in the material removal mechanism.

4.6. *Comparison between MJP and other post-process finishing methods*

In order to demonstrate the advantages of MJP, the comparison between MJP and other popular post-process finishing methods based on some typical indicators is summarized in Table 3. Through the comparison, it is noted that the MJP can obtain nanometric surface roughness on AMed alloy surface, while other processes can hardly obtain the surface roughness smaller than Sa 0.1 μm. Even though shape adaptive grinding method can obtain the surface roughness as low as 3 nm on AMed Ti6Al4V alloy, the polishing tool can hardly adapt to the complicated freeform surfaces, especially for the surface with micro cavities or structures.

In addition to the low surface roughness, MJP can be used on a wide range of materials, including alloys, glass, and ceramics. And it can be used for the polishing of external surface with extremely complicated geometry, due to the highly flexibility of the fluid jet. And for some internal surface with large size, it can also be polished using MJP according to our previous research [81]. Moreover, MJP has much higher form maintainability as compared to most of the current popular

Table 3 – Comparison of multi-jet post polishing (MJP) to other post-process finishing processes[a,b].

Methods		Material applicability	Adaptability to complicated external surface	Applicability to internal surface	Form maintainability	Surface roughness can be obtained on AMed alloy surface	References
Multi-jet Polishing		Wide	High	Medium	High	Sa 30 nm, or smaller using finer abrasive	[48,49]
Traditional machining method	Grinding /Milling	**Wide**	Low	Low	**High**	Sa <0.2 μm [59]	[59–61]
	Burnishing	Narrow	Low	Medium	Medium	Sa <0.1 μm [59]	[59,62,63]
Mechanical removal method induced by abrasive or small particle	Mass Finishing	**Wide**	High	Medium	Low	Ra 0.9 μm [64]	[64–66]
	Shape adaptive Grinding	**Wide**	Medium	Low	**High**	**Ra 3 nm** [24]	[24,67,68]
	Magnetic field assisted finishing	Narrow	Medium-High	Medium	Medium	Sa 0.15 μm [69]	[37,,69,70]
	Abrasive Flow Machining	**Wide**	Medium	**High**	Low	Ra 1.3 μm [21]	[20,21]
	Sand blasting /shot peening	**Wide**	High	Low	Low	Ra 0.19 μm [71]	[15–17,71]
High energy beam method	Laser polishing	**Wide**	High	Low	Medium	Ra 0.1 μm [72]	[72–76]
	Electron-beam irradiation	Medium	High	Low	**High**	Sa 0.5 μm [30]	[30]
Chemical/electrochemical	Electrochemical polishing	Narrow	High	**High**	Low	Sa 1.7 μm [77]	[11,77–79]
	Chemical polishing	Narrow	High	**High**	Low	Ra 1 μm [80]	[31,80]

Note: Bold items are usually regarded as advantages. [a]These characteristics are mainly considered when evaluating a postprocess finishing process. [b] This is only a general comparison and these characteristics may vary for specific tools.

finishing methods, including mass finishing, and electrochemical/chemical polishing.

5. Conclusions

Post-process finishing is still a challenging issue for the extending the applications of additive manufacturing. A multi-jet post polishing (MJP) process is proposed for the post-process finishing of powder bed fusion (PBF) 316L stainless steel (SS) in this paper. The finishing performance of MJP on PBF 316L SS has been demonstrated through a group of systematic experiments, as well as the investigation on the polishing performance. The following conclusions can be drawn based on the experimental results.

(1) MJP is effective for the post-process finishing of PBF 316L SS, which can obtain nanometric surface roughness together with high form accuracy. The surface roughness in Sa was reduced from 2.269 μm to 0.030 μm after MJP, while it was reduced from 26.02 μm to 0.874 μm in Sz.
(2) MJP can successfully remove the surface defects on the PBF 316L SS, including partially melted or melted particles, laser melting marks, debris, and cracks.
(3) The microhardness of PBF 316L SS can be increased after MJP on the top surface. However, the hardness increasement depth is not larger than 1 μm. Moreover, there is no obvious effect on the microhardness of the side surface after MJP.
(4) There is no obvious influence of MJP on the surface microstructure, surface composition and material phase of PBF 316L SS.
(5) Within appropriate working pressure range, higher fluid pressure can obtain higher material removal rate, so as to obtain better surface roughness. Smaller scanning interval and feed rate can obtain better surface roughness induced by longer polishing time. No obvious effect of the stand-off distance to the surface roughness is found in MJP.

CRediT authorship contribution statement

Chunjin Wang: Conceptualization, Methodology, Formal analysis, Investigation, Writing – original draft, Funding acquisition. **Yee Man Loh:** Methodology, Investigation, Validation. **Chi Fai Cheung:** Conceptualization, Methodology, Supervision, Funding acquisition, Project administration, Writing – review & editing, Resources. **Xiaoliang Liang:** Methodology, Investigation. **Zili Zhang:** Investigation, Validation. **Lai Ting Ho:** Investigation, Writing – review & editing.

Declaration of Competing Interest

The authors declare that they have no known competing financial interests or personal relationships that could have appeared to influence the work reported in this paper.

Acknowledgements

The work described in this paper was mainly supported by General Research Fund from the Research Grants Council (Project No.: 15200119) and Innovation and Technology Commission (ITC) (Project No.: ITS/076/18FP) of Hong Kong Special Administrative Region (HKSAR), China. The authors would also like to express their sincerely thanks to the financial support from the Research and Innovation Office of The Hong Kong Polytechnic University (project code: BD9B, BBXL, BBX5) and the research studentship (Project codes: RH3Y).

REFERENCES

[1] Gu D, Shi X, Poprawe R, Bourell DL, Setchi R, Zhu J. Material-structure-performance integrated laser-metal additive manufacturing. Science 2021;372(6545):eabg1487.
[2] Sun Z, Fan Z, Tian Y, Prakash C, Guo J, Li L. Post-processing of additively manufactured microstructures using alternating-magnetic field-assisted finishing. J Mater Res Technol 2022;19:1922–33.
[3] Sanchez S, Smith P, Xu Z, Gaspard G, Hyde CJ, Wits WW, et al. Powder Bed Fusion of nickel-based superalloys: a review. Int J Mach Tool Manufact 2021;165:103729.
[4] Stern ML, Bari JM. A novel method for fabricating additive manufactured lightweight, optical quality metallic mirrors. MIT Lincoln Laboratory Lexington United States; 2016.
[5] Morris Technologies. http://www.morristech.com/.
[6] Biyik S, Arslan F, Aydin M. Arc-erosion behavior of boric oxide-reinforced silver-based electrical contact materials produced by mechanical alloying. J Electron Mater 2015;44(1):457–66.
[7] Biyik S, Aydin M. Fabrication and arc-erosion behavior of Ag_8SnO_2 electrical contact materials under inductive loads. Acta Phys Pol, A 2017;131(3):339–42.
[8] Guler O, Varol T, Alver U, Biyik S. The wear and arc erosion behavior of novel copper based functionally graded electrical contact materials fabricated by hot pressing assisted electroless plating. Adv Powder Technol 2021;32(8):2873–90.
[9] Bandyopadhyay A, Krishna B, Xue W, Bose S. Application of laser engineered net shaping (LENS) to manufacture porous and functionally graded structures for load bearing implants. J Mater Sci Mater Med 2009;20(1):29.
[10] Maleki E, Bagherifard S, Bandini M, Guagliano M. Surface post-treatments for metal additive manufacturing: progress, challenges, and opportunities. Addit Manuf 2021;37:101619.
[11] Pathak S, Zulić S, Kaufman J, Kopeček J, Stránský O, Böhm M, et al. Post-processing of selective laser melting manufactured SS-304L by laser shock peening. J Mater Res Technol 2022;19:4787–92.
[12] Limbasiya N, Jain A, Soni H, Wankhede V, Krolczyk G, Sahlot P. A comprehensive review on the effect of process parameters and post-process treatments on microstructure and mechanical properties of selective laser melting of AlSi10Mg. J Mater Res Technol 2022;21:1141–76.
[13] Kim EJ, Lee CM, Kim DH. The effect of post-processing operations on mechanical characteristics of 304L stainless steel fabricated using laser additive manufacturing. J Mater Res Technol 2021;15:1370–81.
[14] Zhang L, Yuan Z, Qi Z, Cai D, Cheng Z, Qi H. CFD-based study of the abrasive flow characteristics within constrained flow passage in polishing of complex titanium alloy surfaces. Powder Technol 2018;333:209–18.
[15] Rossi S, Deflorian F, Venturini F. Improvement of surface finishing and corrosion resistance of prototypes produced by direct metal laser sintering. J Mater Process Technol 2004;148(3):301–9.
[16] AlMangour B, Yang JM. Improving the surface quality and mechanical properties by shot-peening of 17-4 stainless steel fabricated by additive manufacturing. Mater Des 2016;110:914–24.
[17] Wen P, Voshage M, Jauer L, Chen Y, Qin Y, Poprawe R, et al. Laser additive manufacturing of Zn metal parts for biodegradable applications: processing, formation quality and mechanical properties. Mater Des 2018;155:36–45.
[18] Damon J, Dietrich S, Vollert F, Gibmeier J, Schulze V. Process dependent porosity and the influence of shot peening on porosity morphology regarding selective laser melted AlSi10Mg parts. Addit Manuf 2018;20:77–89.
[19] Furumoto T, Ueda T, Amino T, Hosokawa A. A study of internal face finishing of the cooling channel in injection mold with free abrasive grains. J Mater Process Technol 2011;211(11):1742–8.
[20] Mohammadian N, Turenne S, Brailovski V. Surface finish control of additively-manufactured Inconel 625 components using combined chemical-abrasive flow polishing. J Mater Process Technol 2018;252:728–38.
[21] Guo J, Song C, Fu Y, Au KH, Kum CW, Goh MH, et al. Internal surface quality enhancement of selective laser melted Inconel 718 by abrasive flow machining. J Manuf Sci Eng 2020;142(10):101003.
[22] Schmid M, Simon C, Levy GN. Finishing of SLS-parts for rapid manufacturing (RM) – a comprehensive approach. In: Proceedings of 20th Solid Freeform Fabrication Symposium. 3; 5 August 2009. p. 1–10. Austin.
[23] Boschetto A, Bottini L, Veniali F. Surface roughness and radiusing of Ti6Al4V selective laser melting-manufactured parts conditioned by barrel finishing. Int J Adv Manuf Technol 2018;94(5):2773–90.
[24] Kaynak Y, Kitay O. The effect of post-processing operations on surface characteristics of 316L stainless steel produced by selective laser melting. Addit Manuf 2019;26:84–93.
[25] Beaucamp AT, Namba Y, Charlton P, Jain S, Graziano AA. Finishing of additively manufactured titanium alloy by shape adaptive grinding (SAG). Surf Topogr Metrol Prop 2015;3(2):024001.
[26] Lamikiz A, Sanchez JA, de Lacalle LL, Arana JL. Laser polishing of parts built up by selective laser sintering. Int J Mach Tool Manufact 2007;47(12–13):2040–50.
[27] Marimuthu S, Triantaphyllou A, Antar M, Wimpenny D, Morton H, Beard M. Laser polishing of selective laser melted components. Int J Mach Tool Manufact 2015;95:97–104.
[28] Ma CP, Guan YC, Zhou W. Laser polishing of additive manufactured Ti alloys. Opt Laser Eng 2017;93:171–7.
[29] Vaithilingam J, Goodridge RD, Hague RJM, Christie SDR, Edmondson S. The effect of laser remelting on the surface chemistry of Ti6al4V components fabricated by selective laser melting. J Mater Process Technol 2016;232:1–8.
[30] Narayanan TS, Kim J, Jeong HE, Park HW. Enhancement of the surface properties of selective laser melted maraging steel by large pulsed electron-beam irradiation. Addit Manuf 2020;33:101125.
[31] Pyka G, Burakowski A, Kerckhofs G, Moesen M, Van BS, Schrooten J, et al. Surface modification of Ti6Al4V open porous structures produced by additive manufacturing. Adv Eng Mater 2012;14(6):363–70.
[32] Habibzadeh S, Li L, Shum-Tim D, Davis EC, Omanovic S. Electrochemical polishing as a 316L stainless steel surface treatment method: towards the improvement of biocompatibility. Corrosion Sci 2014;87:89–100.

[33] Zhang BC, Lee XH, Bai JM, Guo JF, Wang P, Sun CN, et al. Study of selective laser melting (SLM) Inconel 718 part surface improvement by electrochemical polishing. Mater Des 2017;116:531–7.
[34] Łyczkowska E, Szymczyk P, Dybała B, Chlebus E. Chemical polishing of scaffolds made of Ti–6Al–7Nb alloy by additive manufacturing. Arch Civ Mech Eng 2014;14(4):586–94.
[35] Crane NB, Ni Q, Ellis A, Hopkinson N. Impact of chemical finishing on laser-sintered nylon 12 materials. Addit Manuf 2017;13:149–55.
[36] Tyagi P, Goulet T, Riso C, Stephenson R, Chuenprateep N, Schlitzer J, et al. Reducing the roughness of internal surface of an additive manufacturing produced 316 steel component by chempolishing and electropolishing. Addit Manuf 2019;25:32–8.
[37] Guo J, Au KH, Sun CN, Goh MH, Kum CW, Liu K, et al. Novel rotating-vibrating magnetic abrasive polishing method for double-layered internal surface finishing. J Mater Process Technol 2019;264:422–37.
[38] Tan KL, Yeo SH. Surface finishing on IN625 additively manufactured surfaces by combined ultrasonic cavitation and abrasion. Addit Manuf 2020;31:100938.
[39] Nagalingam AP, Yuvaraj HK, Yeo SH. Synergistic effects in hydrodynamic cavitation abrasive finishing for internal surface-finish enhancement of additive-manufactured components. Addit Manuf 2020;33:101110.
[40] Yang L, Laugel N, Housden J, Espitalier L, Matthews A, Yerokhin A. Plasma additive layer manufacture smoothing (PALMS) technology—an industrial prototype machine development and a comparative study on both additive manufactured and conventional machined AISI 316 stainless steel. Addit Manuf 2020;34:101204.
[41] Fähnle OW, Van Brug H, Frankena HJ. Fluid jet polishing of optical surfaces. Appl Opt 1998;37(28):6771–3.
[42] Wang C, Zhang Z, Cheung CF, Luo W, Loh YM, Lu Y, et al. Maskless fluid jet polishing of optical structured surfaces. Precis Eng 2022;73:270–83.
[43] Beaucamp A, Namba Y, Freeman R. Dynamic multiphase modeling and optimization of fluid jet polishing process. CIRP annals 2012;61(1):315–8.
[44] Zhao J, Xiang Y, Fan C. A new method for polishing the inner wall of a circular tube with a soft abrasive rotating jet. Powder Technol 2022;398:117068.
[45] Zhang L, Ji R, Fu Y, Qi H, Kong F, Li H, et al. Investigation on particle motions and resultant impact erosion on quartz crystals by the micro-particle laden waterjet and airjet. Powder Technol 2020;360:452–61.
[46] Qi H, Wen D, Yuan Q, Zhang L, Chen Z. Numerical investigation on particle impact erosion in ultrasonic-assisted abrasive slurry jet micro-machining of glasses. Powder Technol 2017;314:627–34.
[47] Beaucamp A, Katsuura T, Kawara Z. A novel ultrasonic cavitation assisted fluid jet polishing system. CIRP Annals 2017;66(1):301–4.
[48] Wang CJ, Cheung CF, Ho LT, Liu MY, Lee WB. A novel multi-jet polishing process and tool for high-efficiency polishing. Int J Mach Tool Manufact 2017;115:60–73.
[49] Cheung CF, Wang C, Ho LT, Chen J. Curvature-adaptive multi-jet polishing of freeform surfaces. CIRP Annals 2018;67(1):357–60.
[50] Cao ZC, Cheung CF. Theoretical modelling and analysis of the material removal characteristics in fluid jet polishing. Int J Mech Sci 2014;89:158–66.
[51] Zhang Q, Duan B, Zhang Z, Wang J, Si C. Effect of ultrasonic shot peening on microstructure evolution and corrosion resistance of selective laser melted Ti–6Al–4V alloy. J Mater Res Technol 2021;11:1090–9.
[52] Uzan NE, Ramati S, Shneck R, Frage N, Yeheskel O. On the effect of shot-peening on fatigue resistance of AlSi10Mg specimens fabricated by additive manufacturing using selective laser melting (AM-SLM). Addit Manuf 2018;21:458–64.
[53] Yusuf SM, Nie M, Chen Y, Yang S, Gao N. Microstructure and corrosion performance of 316L stainless steel fabricated by Selective Laser Melting and processed through high-pressure torsion. J Alloys Compd 2018;763:360–75.
[54] Sun Z, Tan X, Tor SB, Yeong WY. Selective laser melting of stainless steel 316L with low porosity and high build rates. Mater Des 2016;104:197–204.
[55] Wang C, Cheung CF, Liu M, Lee WB. Fluid jet-array parallel machining of optical microstructure array surfaces. Opt Express 2017;25(19):22710–25.
[56] Wang CJ, Cheung CF, Ho LT, Loh YM. An investigation of effect of stand-off distance on the material removal characteristics and surface generation in fluid jet polishing. Nanomanuf and Metro 2020;3(2):112–22.
[57] Natarajan Y, Murugesan PK, Mohan M, Khan SA. Abrasive Water Jet Machining process: a state of art of review. J Manuf Process 2020;49:271–322.
[58] Axinte DA, Karpuschewski B, Kong MC, Beaucamp AT, Anwar S, Miller D, et al. High energy fluid jet machining (HEFJet-Mach): from scientific and technological advances to niche industrial applications. CIRP Annals 2014;63(2):751–71.
[59] Raaj RK, Anirudh PV, Karunakaran C, Kannan C, Jahagirdar A, Joshi S, et al. Exploring grinding and burnishing as surface post-treatment options for electron beam additive manufactured Alloy 718. Surf Coating Technol 2020;397:126063.
[60] Lizzul L, Sorgato M, Bertolini R, Ghiotti A, Bruschi S. Surface finish of additively manufactured Ti6Al4V workpieces after ball end milling. Procedia CIRP 2021;102:228–33.
[61] Lizzul L, Sorgato M, Bertolini R, Ghiotti A, Bruschi S. Ball end milling machinability of additively and conventionally manufactured Ti6Al4V tilted surfaces. J Manuf Process 2021;72:350–60.
[62] de Bruijn AC, Gómez-Gras G, Pérez MA. On the effect upon the surface finish and mechanical performance of ball burnishing process on fused filament fabricated parts. Addit Manuf 2021;46:102133.
[63] Salmi M, Huuki J, Ituarte IF. The ultrasonic burnishing of cobalt-chrome and stainless steel surface made by additive manufacturing. Progress Add Manuf 2017;2(1):31–41.
[64] Bagehorn S, Wehr J, Maier HJ. Application of mechanical surface finishing processes for roughness reduction and fatigue improvement of additively manufactured Ti-6Al-4V parts. Int J Fatig 2017;102:135–42.
[65] Khorasani M, Ghasemi AH, Farabi E, Leary M, Gibson I, Rolfe B. A comprehensive investigation of abrasive barrel finishing on hardness and manufacturability of laser-based powder bed fusion hollow components. Int J Adv Manuf Technol 2022;120(5):3471–90.
[66] Khan HM, Sirin TB, Tarakci G, Bulduk ME, Coskun M, Koc E, et al. Improving the surface quality and mechanical properties of selective laser sintered PA2200 components by the vibratory surface finishing process. SN Appl Sci 2021;3(3):1–4.
[67] Beaucamp A, Namba Y, Combrinck H, Charlton P, Freeman R. Shape adaptive grinding of CVD silicon carbide. CIRP annals 2014;63(1):317–20.
[68] Zhu WL, Jain C, Han Y, Beaucamp A. Predictive topography model for shape adaptive grinding of metal matrix composites. CIRP Annals 2021;70(1):269–72.
[69] Yamaguchi H, Fergani O, Wu PY. Modification using magnetic field-assisted finishing of the surface roughness

and residual stress of additively manufactured components. CIRP Annals 2017;66(1):305–8.
[70] Zhang J, Chaudhari A, Wang H. Surface quality and material removal in magnetic abrasive finishing of selective laser melted 316L stainless steel. J Manuf Process 2019;45:710–9.
[71] Bagherifard S, Slawik S, Fernández-Pariente I, Pauly C, Mücklich F, Guagliano M. Nanoscale surface modification of AISI 316L stainless steel by severe shot peening. Mater Des 2016;102:68–77.
[72] Zhihao F, Libin L, Longfei C, Yingchun G. Laser polishing of additive manufactured superalloy. Procedia Cirp 2018;71:150–4.
[73] Chen L, Richter B, Zhang X, Ren X, Pfefferkorn FE. Modification of surface characteristics and electrochemical corrosion behavior of laser powder bed fused stainless-steel 316L after laser polishing. Addit Manuf 2020;32:101013.
[74] Cui M, Lu L, Zhang Z, Guan Y. A laser scanner–stage synchronized system supporting the large-area precision polishing of additive-manufactured metallic surfaces. Eng 2021;7(12):1732–40.
[75] Park SH, Liu P, Yi K, Choi G, Jhang KY, Sohn H. Mechanical properties estimation of additively manufactured metal components using femtosecond laser ultrasonics and laser polishing. Int J Mach Tool Manufact 2021;166:103745.
[76] Obeidi MA, Mussatto A, Dogu MN, Sreenilayam SP, McCarthy E, Ahad IU, et al. Laser surface polishing of Ti-6Al-4V parts manufactured by laser powder bed fusion. Surf Coating Technol 2022;434:128179.
[77] Lynch ME, Williams K, Cabrera M, Beccuti T. Surface finishing of additively manufactured IN718 lattices by electrochemical machining. Int J Adv Manuf Technol 2021;113(3):967–84.
[78] Han W, Fang F. Orientation effect of electropolishing characteristics of 316L stainless steel fabricated by laser powder bed fusion. Front Mech Eng 2021;16(3):580–92.
[79] Zhao C, Qu N, Tang X. Confined electrochemical finishing of additive-manufactured internal holes with coaxial electrolyte flushing. J Electrochem Soc 2021;168(11):113504.
[80] Raikar S, Heilig M, Mamidanna A, Hildreth OJ. Self-terminating etching process for automated support removal and surface finishing of additively manufactured Ti-6Al-4 V. Addit Manuf 2021;37:101694.
[81] Cheung CF, Wang CJ, Cao ZC, Ho LT, Liu MY. Development of a multi-jet polishing process for inner surface finishing. Precis Eng 2018;52:112–21.